

Broadband Spectral Fitting of Blazars using XSPEC

S. Sahayanathan¹, A. Sinha² and R. Misra²

¹ Astrophysical Sciences Division, Bhabha Atomic Research Centre, Mumbai - 400085, India;
sunder@barc.gov.in

² Inter-University Center for Astronomy and Astrophysics, Post Bag 4, Pune, India

Abstract The broadband spectral energy distribution (SED) of blazars is generally interpreted as radiation arising from synchrotron and inverse Compton mechanisms. Traditionally, the underlying source parameters responsible for these emission processes, like particle energy density, magnetic field, etc., are obtained through simple visual reproduction of the observed fluxes. However, this procedure is incapable of providing the confidence range on the estimated parameters. In this work, we propose an efficient algorithm to perform a statistical fit of the observed broadband spectrum of blazars using different emission models. Moreover, in this work we use the observable quantities as the fit parameters, rather than the direct source parameters which govern the resultant SED. This significantly improves the convergence time and eliminates the uncertainty regarding the initial guess parameters. This approach also has an added advantage of identifying the degenerate parameters, which can be removed by including more observable information and/or additional constraints. A computer code developed based on this algorithm is implemented as an user-defined routine in the standard X-ray spectral fitting package, XSPEC. Further, we demonstrate the efficacy of the algorithm by fitting the well sampled SED of the blazar, 3C 279, during its gamma ray flare in 2014.

Key words: galaxies: active–BL Lacertae objects: general– quasars: individual(3C 279)
 – relativistic processes–radiation mechanisms: non-thermal

1 INTRODUCTION

A presence of powerful jets is one of the striking features of active galactic nuclei (AGN), with blazars belonging to a special class where the jet is aligned close to the line of sight (Antonucci 1993; Urry & Padovani 1995). The emission from blazars is predominantly non-thermal in nature and extends from radio to gamma ray energies (Sambruna et al. 1996). Transparency to high energy gamma rays and a rapidly varying flux implies the jet is relativistic (Dondi & Ghisellini 1995) and hence, its emission is significantly boosted due to relativistic Doppler effects. Besides this non-thermal jet emission, blazar spectral energy distribution (SED) is often observed to have broad emission/absorption lines and thermal features (Francis et al. 1991; Liu & Bai 2006; Malmrose et al. 2011). Consistently, blazars are further subdivided into two classes, namely, flat spectrum radio quasars (FSRQs) with broad line features and BL Lacs with weak or no emission/absorption lines (Padovani et al. 2007).

The broadband SEDs of blazars are characterized by a typical double hump feature which is attributed to radiative losses encountered by a non-thermal electron distribution (Abdo et al. 2010). The low energy component is well understood as synchrotron emission from a relativistic population of electrons in the jet losing its energy in a magnetic field; whereas, the high energy emission is generally attributed to inverse Compton scattering of soft target photons by the same electron distribution. The soft

target photons can be synchrotron photons themselves, commonly referred as synchrotron self Compton (SSC) (Konigl 1981; Marscher & Gear 1985; Ghisellini & Maraschi 1989) and/or the other photon field from the jet environment, commonly referred as external Compton (EC) (Begelman & Sikora 1987; Melia & Konigl 1989; Dermer et al. 1992). The most prominent external photon fields which are scattered off by the jet electrons via inverse Compton process are the emission from the accretion disk (EC/disk) (Dermer & Schlickeiser 1993; Boettcher et al. 1997), the reprocessed broad emission lines from broad line emitting regions (EC/BLR) (Sikora et al. 1994; Ghisellini & Madau 1996) and the thermal infrared radiation from the dusty torus (EC/IR), proposed by the unification theory (Sikora et al. 1994; Błażejowski et al. 2000; Ghisellini & Tavecchio 2009). The relative contributions of these emission processes are usually obtained by simple visual reproduction of the broadband SED using various emissivity functions (Paliya et al. 2015; Sahayanathan & Godambe 2012; Kushwaha et al. 2013; Ghisellini & Tavecchio 2009). However, a proper statistical treatment of the broadband SED considering these emission processes has not been pursued in detail, except for a few recent works (e.g. Mankuzhiyil et al. 2011; Zhang et al. 2012; Kang et al. 2014). Such a statistical treatment, besides providing the range of source parameters which is consistent with the observation, will also benefit us in understanding the jet environment and the possible location of the emission region (Zhang et al. 2012, 2013, 2014, 2015).

The present epoch is particularly rewarding for observational astronomy due to some remarkable technological advancements in recent years. This has resulted in high sensitivity experiments operating at various energy bands like, optical (e.g. *Hubble Space Telescope*), X-ray (e.g. *Swift*, *NuSTAR*, *AstroSat*) and gamma rays (e.g. *Fermi*, *MAGIC*, *VERITAS*, *HESS*). With the availability of high quality data from these experiments through coordinated multi wavelength observations, we now have rich spectral information of blazars during flare as well as quiescent flux states (Carnerero et al. 2015; Aleksić et al. 2015; Abdo et al. 2011; Sinha et al. 2016). This development, in turn, demands more sophisticated spectral fitting numerical codes, involving various physical emission models rather than simple mathematical functions representing a narrow range of energies (Sinha et al. 2015; Bhagwan et al. 2014; Rani et al. 2013), which are capable of extracting the source parameters of blazars with significant confidence levels. Successful reproduction of blazar SED during quiescent and different flaring states using such spectral fitting algorithms will help us in understanding the physics behind blazar flares and its dynamics (Paliya et al. 2015; Kushwaha et al. 2014; Ghisellini & Tavecchio 2009).

The main challenge encountered while developing the algorithms for broadband spectral fitting of blazars, involving different physical emission models, is the numerical intensiveness. The presence of multiple integrations in different emissivity formulae require a large number of nested loops making the algorithms computationally intensive (Mankuzhiyil et al. 2011; Zhang et al. 2012; Kang et al. 2014). In addition, a complex dependence of the source parameters on the observed flux levels makes the algorithms wander considerably in the parameter space, eventually slowing down the fitting process (Rybicki & Lightman 1986; Blumenthal & Gould 1970; Dermer & Schlickeiser 1993). However, thanks to the availability of modern high speed computers with multi core processors and optimized numerical algorithms directed towards effective utilization of resources, one can now perform this spectral fitting procedure relatively faster.

The attempt to perform a statistical fitting of blazar SED was first initiated by Mankuzhiyil et al. (2011), where the authors fitted the multi-epoch, broadband SED of Mrk 421 using synchrotron and SSC processes. The fitting was performed using χ^2 minimization technique incorporating Levenberg-Marquardt algorithm (Press et al. 1992). For such algorithms, convergence to the actual minima is strongly dependent on the initial guess values of the source parameters. However, the non-linear dependence of the source parameters with different emissivity functions often makes it hard/impossible to choose the right set of initial guess values to begin with. This may eventually lead the minimization algorithm to descent towards unphysical parameter space. Alternatively, a novel approach was proposed by Zhang et al. (2012) where the authors used the observed information to extract most of the source parameters (Tavecchio et al. 1998). The source magnetic field and the jet Doppler factor are finally obtained through χ^2 minimization. This approach has significantly eased the problem of choosing the initial guess values. Recently, Kang et al. (2014) added EC/IR and EC/BLR processes along with synchrotron and SSC processes and performed a spectral fitting for the SED of 28 low energy peaked BL

Lac objects. For each source, they generated the SED corresponding to broad range of parameters and calculated the χ^2 . The best fit parameters and their errors were estimated from this χ^2 space. However, such algorithms are inefficient and excessive computational time forced the authors to freeze certain parameters.

In this work, we develop an algorithm considering synchrotron, SSC and EC mechanisms, to fit the broadband SED of blazars using the standard X-ray spectral fitting package *XSPEC* (Arnaud 1996). *XSPEC* is primarily developed to obtain the X-ray fluxes from the source by convolving a source spectral model function with the detector response matrix of the satellite based X-ray telescopes. It employs the Levenberg-Marquardt algorithm to fit the observed photon counts with the model spectrum and produce the “most probable” flux of the source. The software package also provides the flexibility to add user defined spectral models (local models) and fit with the observed photon counts. We developed separate additive local models for synchrotron, SSC and EC processes which can be added according to the necessity. Rather than fitting the direct source parameters governing the underlying spectrum, we fit the observed spectrum. This ensures faster convergence and removes the problem of guessing initial values. The numerical codes for various emissivities are significantly optimized to reduce the machine run time. An added advantage of using *XSPEC* spectral fitting package, besides being well optimized and widely tested, is that it allows us to fit the photon counts within the energy bins rather than the fluxes at their mean energy. The *XSPEC* routines are finally applied on the well studied FSRQ, 3C 279, as a test case. The choice of 3C 279 is mainly driven by the fact that the non-thermal emission dominates its entire SED, availability of sufficient multi wavelength data and the need for EC process to reproduce its gamma ray observation (Sahayanathan & Godambe 2012).

The paper is organised as follows: in Section 2, we describe the different emission models relevant for the broadband spectral fitting of the non thermal emission from blazars. Here, we derive the emissivity formulae for the synchrotron and inverse Compton processes and show their relation with the observed spectral information. In Section 3, we present the proposed spectral fitting procedure using *XSPEC* and its application on 3C 279, and in Section 4, we discuss the implications and advantages of the developed spectral fitting algorithm. A cosmology with $\Omega_m = 0.3$, $\Omega_\Lambda = 0.7$ and $H_0 = 70 \text{ km s}^{-1} \text{ Mpc}^{-1}$ is used in this work.

2 BLAZAR JET EMISSION MODELS

We model the non-thermal emission from the blazar jet to originate from a spherical region of radius R , moving down the jet with bulk Lorentz factor Γ at an angle θ with respect to the line of sight of the observer. The emission region is filled with a broken power law electron distribution, given by

$$N(\gamma) d\gamma = \begin{cases} K \gamma^{-p} d\gamma & \text{for } \gamma_{\min} < \gamma < \gamma_b \\ K \gamma_b^{q-p} \gamma^{-q} d\gamma & \text{for } \gamma_b < \gamma < \gamma_{\max} \end{cases} \text{ cm}^{-3} \quad (1)$$

undergoing synchrotron loss due to a tangled magnetic field, B , and inverse Compton losses by scattering off low energy photons. Here, $\gamma (= \frac{E}{m_e c^2})$ is the dimensionless energy with m_e the mass of electron and c being the velocity of light, K the normalisation factor, γ_b is the break energy and p and q are the low and high energy electron spectral indices. The target photons for the inverse Compton scattering are synchrotron photons (SSC) and an isotropic blackbody photon field at temperature T_* external to jet ¹.

¹ Quantities with subscript * are measured in the co-moving frame where the parent galaxy is at rest; whereas, the rest of the quantities are measured in emission region frame where the electron distribution is homogeneous, unless mentioned otherwise.

2.1 Synchrotron Specific Intensity

The synchrotron emissivity due to an isotropic electron distribution losing its energy in a tangled magnetic field, B , is given by (Rybicki & Lightman 1986)

$$j_{\text{syn}}(\nu) = \frac{1}{4\pi} \int_{\gamma_{\min}}^{\gamma_{\max}} P_{\text{syn}}(\gamma, \nu) N(\gamma) d\gamma \quad \text{erg/cm}^3/\text{s/Hz/Sr} \quad (2)$$

where, $P_{\text{syn}}(\gamma, \nu)$ is the pitch angle averaged single particle emissivity, given by

$$P_{\text{syn}}(\gamma, \nu) = \frac{\sqrt{3}\pi e^3 B}{4m_e c^2} F\left(\frac{\nu}{\nu_c}\right) \quad \text{erg/s/Hz} \quad (3)$$

with,

$$\nu_c = \frac{3\gamma^2 e B}{16m_e c} \quad \text{Hz} \quad (4)$$

and synchrotron power function (Melrose 1980)

$$F(x) = x \int_x^\infty K_{5/3}(\xi) d\xi \approx 1.8 x^{1/3} e^{-x} \quad (5)$$

Here, $K_{5/3}$ is the modified Bessel function of order 5/3. The function $F(x)$ has a single peak at $x \approx 0.29$. At the optically thick regime, synchrotron photons are self absorbed and the absorption coefficient is given by (Ghisellini & Svensson 1991; Chiaberge & Ghisellini 1999)

$$\kappa(\nu) = -\frac{1}{8\pi m_e \nu^2} \int_{\gamma_{\min}}^{\gamma_{\max}} \frac{N(\gamma)}{\gamma \sqrt{\gamma^2 - 1}} \frac{d}{d\gamma} \left[\gamma \sqrt{\gamma^2 - 1} P_{\text{syn}}(\gamma, \nu) \right] \quad \text{cm}^{-1} \quad (6)$$

Using the emissivity and absorption coefficient, equation (2) and (6), the synchrotron specific intensity can be obtained from the radiative transfer equation as (Rybicki & Lightman 1986)

$$I_{\text{syn}}(\nu) = \frac{j_{\text{syn}}(\nu)}{\kappa(\nu)} \left[1 - e^{-\kappa(\nu) R} \right] \quad \text{erg/cm}^2/\text{s/Hz/Sr} \quad (7)$$

For optically thin regime, $I_{\text{syn}}(\nu) \approx j_{\text{syn}}(\nu) R$.

Alternatively, an approximate analytical solution of the synchrotron emissivity can be obtained by assuming the single particle emissivity as (Shu 1991)

$$P_{\text{syn}}(\gamma, \nu) = \frac{4}{3} \beta^2 \gamma^2 c \sigma_T U_B \Phi_\nu(\gamma) \quad (8)$$

where, $\beta (= \frac{v}{c})$ is the dimensionless velocity of the emitting electron, σ_T is the Thomson cross section and the spectral function $\Phi_\nu(\gamma)$ satisfies the relation

$$\int_0^\infty \Phi_\nu(\gamma) d\gamma = 1 \quad (9)$$

In case of synchrotron emissivity due to non-thermal distribution of electrons, the narrow shape of $F(x)$ let us approximate the function $\Phi_\nu(\gamma)$ as a δ -function

$$\Phi_\nu(\gamma) \rightarrow \delta(\nu - \gamma^2 \nu_L) \quad (10)$$

where, the Larmor frequency $\nu_L = \frac{eB}{2\pi m_e c}$. Using this approximation on equation (8) and the δ -function property

$$\delta[f(x)] = \sum_i \frac{\delta(x - x_i)}{\left| \frac{df}{dx} \right|_{x=x_i}} \quad (11)$$

with x_i 's being the roots of $f(x)$, the synchrotron emissivity can be obtained as as² (Sahayanathan & Godambe 2012)

$$\tilde{j}_{\text{syn}}(\nu) \approx \frac{\sigma_T c B^2}{48\pi^2} \nu_L^{-\frac{3}{2}} N \left(\sqrt{\frac{\nu}{\nu_L}} \right) \nu^{\frac{1}{2}} \quad \text{erg/cm}^3/\text{s/Hz/Sr} \quad (12)$$

2.2 SSC Emissivity

The polarization angle averaged differential Compton cross section, in the rest frame of the scattering electron³, is given by the Klein-Nishina formula (Blumenthal & Gould 1970)

$$\frac{d^2\sigma}{d\nu'_s d\Omega'_s} = \frac{r_e^2}{2} \left(\frac{\nu'_s}{\nu'_i} \right)^2 \left(\frac{\nu'_i}{\nu'_s} + \frac{\nu'_s}{\nu'_i} - 1 + \cos\psi'^2 \right) \delta \left[\nu'_s - \frac{\nu'_i}{1 + \frac{h\nu'_i}{m_e c^2} (1 - \cos\psi')} \right] \quad \text{cm}^2/\text{Sr/Hz} \quad (13)$$

where, ν'_i and ν'_s are the frequency of the incident and the scattered photon, ψ' is the angle between their direction, h is the Planck's constant and r_e is the classical electron radius. For the case of elastic scattering, $\nu'_s \approx \nu'_i$ and the equation (13) reduces to the classical Thomson limit

$$\frac{d^2\sigma}{d\nu'_s d\Omega'_s} \approx \frac{r_e^2}{2} (1 + \cos\psi'^2) \delta(\nu'_s - \nu'_i) \quad (14)$$

The single particle Compton emissivity due to scattering of the isotropic synchrotron photons can then be obtained from Klein-Nishina formula as (Blumenthal & Gould 1970; Jones 1968)

$$P_{\text{ssc}}(\gamma, \nu_s) = \frac{3\pi\sigma_T\nu_s}{\gamma^2} \int_{x_1}^{x_2} \frac{I_{\text{syn}}(\nu_i)}{\nu_i^2} f(\nu_i, \nu_s, \gamma) d\nu_i \quad \text{erg/s/Hz} \quad (15)$$

where,

$$x_1 = \text{MAX} \left[\nu_{\text{syn}}^{\min}, \frac{\nu_s}{4\gamma^2 \left(1 - \frac{h\nu_s}{\gamma m_e c^2} \right)} \right]; \quad \nu_{\text{syn}}^{\min} \approx 1.29 \times 10^6 \gamma_{\min}^2 B \quad (16)$$

$$x_2 = \text{MIN} \left[\nu_{\text{syn}}^{\max}, \frac{\nu_s}{\left(1 - \frac{h\nu_s}{\gamma m_e c^2} \right)} \right]; \quad \nu_{\text{syn}}^{\max} \approx 1.29 \times 10^6 \gamma_{\max}^2 B \quad (17)$$

and

$$f(\nu_i, \nu_s, \gamma) = 2q \log q + (1 + 2q)(1 - q) + \frac{(\zeta q)^2(1 - q)}{2(1 + \zeta q)} \quad (18)$$

² \sim hat represents approximate analytical estimates

³ Quantities with prime are measured in the electron rest frame

with

$$\zeta = \frac{4\gamma h\nu_i}{m_e c^2} \quad \text{and} \quad q = \frac{\nu_s}{4\nu_i \gamma^2 \left(1 - \frac{h\nu_s}{\gamma m_e c^2}\right)}$$

Finally, the SSC emissivity due to the electron distribution given in equation (1) will be

$$j_{\text{ssc}}(\nu) = \frac{1}{4\pi} \int_{\gamma_{\min}}^{\gamma_{\max}} P_{\text{ssc}}(\gamma, \nu) N(\gamma) d\gamma \quad \text{erg/cm}^3/\text{s/Hz/Sr} \quad (19)$$

Similar to the synchrotron case, an approximate analytical solution of SSC emissivity, happening in the Thomson regime, can be obtained by considering the single particle emissivity as (Sahayanathan & Godambe 2012)

$$P_{\text{ssc}}(\gamma, \nu) = \frac{4}{3} \beta^2 \gamma^2 c \sigma_T \int_{\nu_{\text{syn}}^{\min}}^{\nu_{\text{syn}}^{\max}} U(\xi) d\xi \Psi_{\nu}(\xi, \gamma) \quad (20)$$

where,

$$U_{\text{ph}} = \int_{\nu_{\text{syn}}^{\min}}^{\nu_{\text{syn}}^{\max}} U(\xi) d\xi \quad \text{erg/cm}^3 \quad (21)$$

is the energy density of the synchrotron photons and the function $\Psi_{\nu}(\xi, \gamma)$ satisfies the condition

$$\int_0^{\infty} \Psi_{\nu}(\xi, \gamma) d\nu = 1 \quad (22)$$

Since the scattered photon frequency in the Thomson regime is $\gamma^2 \xi$ approximately, we can express $\Psi_{\nu}(\xi, \gamma)$ as

$$\Psi_{\nu}(\xi, \gamma) \rightarrow \delta(\nu - \gamma^2 \xi) \quad (23)$$

From equation (19), the SSC emissivity will then be

$$\tilde{j}_{\text{ssc}}(\nu) \approx \frac{1}{3\pi} c \sigma_T \int_{\gamma_{\min}}^{\gamma_{\max}} U\left(\frac{\nu}{\gamma^2}\right) N(\gamma) d\gamma$$

Expressing $U(\nu) = \frac{4\pi R}{c} j_{\text{syn}}(\nu)$ and using equation (12) we get

$$\tilde{j}_{\text{ssc}}(\nu) \approx \frac{Rc}{36\pi^2} \sigma_T^2 B^2 \nu_L^{-\frac{3}{2}} \nu^{\frac{1}{2}} \int_{\gamma_{\min}}^{\gamma_{\max}} \frac{d\gamma}{\gamma} N\left(\frac{1}{\gamma} \sqrt{\frac{\nu}{\nu_L}}\right) N(\gamma) \quad (24)$$

For the case of non-thermal electron distribution, given by equation (1), we obtain

$$\tilde{j}_{\text{ssc}}(\nu) \approx \frac{Rc}{36\pi^2} K^2 \sigma_T^2 B^2 \nu_L^{-\frac{3}{2}} \nu^{\frac{1}{2}} f(\nu) \quad (25)$$

Here,

$$\begin{aligned}
 f(\nu) = & \left[\left(\frac{\nu}{\nu_L} \right)^{-\frac{p}{2}} \log \left(\frac{\gamma_1}{\gamma_2} \right) + \frac{\gamma_b^{(q-p)}}{q-p} \left(\frac{\nu}{\nu_L} \right)^{-\frac{q}{2}} \right. \\
 & \times (\gamma_1^{(q-p)} - \gamma_{\min}^{(q-p)}) \Theta \left(\frac{1}{\gamma_b} \sqrt{\frac{\nu}{\nu_L}} - \gamma_{\min} \right) \left. \right] \Theta(\gamma_2 - \gamma_1) \\
 & + \left[\gamma_b^{2(q-p)} \left(\frac{\nu}{\nu_L} \right)^{-\frac{q}{2}} \log \left(\frac{\gamma_4}{\gamma_3} \right) + \frac{\gamma_b^{(q-p)}}{q-p} \left(\frac{\nu}{\nu_L} \right)^{-\frac{p}{2}} \right. \\
 & \times (\gamma_4^{(p-q)} - \gamma_{\max}^{(p-q)}) \Theta \left(\gamma_{\max} - \frac{1}{\gamma_b} \sqrt{\frac{\nu}{\nu_L}} \right) \left. \right] \Theta(\gamma_4 - \gamma_3)
 \end{aligned} \tag{26}$$

with Θ being the Heaviside function and

$$\begin{aligned}
 \gamma_1 &= \text{MAX} \left(\gamma_{\min}, \frac{1}{\gamma_b} \sqrt{\frac{\nu}{\nu_L}} \right) \\
 \gamma_2 &= \text{MIN} \left(\gamma_b, \frac{1}{\gamma_{\min}} \sqrt{\frac{\nu}{\nu_L}} \right) \\
 \gamma_3 &= \text{MAX} \left(\gamma_b, \frac{1}{\gamma_{\max}} \sqrt{\frac{\nu}{\nu_L}} \right) \\
 \gamma_4 &= \text{MIN} \left(\gamma_{\max}, \frac{1}{\gamma_b} \sqrt{\frac{\nu}{\nu_L}} \right)
 \end{aligned} \tag{27}$$

2.3 EC Emissivity

The EC emissivity for the case of relativistic electrons with $\gamma \gg 1$ can be estimated following the procedure described in [Dermer & Schlickeiser \(1993\)](#) and [Dermer & Menon \(2009\)](#). Under this case, the direction of the scattered photon (Ω_s), in the frame of the emission region, can be approximated to be that of the electron itself and the differential Compton cross section in the emission region frame can be written as

$$\frac{d^2\sigma}{d\nu_s d\Omega_s} = \delta(\Omega_s - \Omega_e) \oint d\Omega'_s \left(\frac{d\nu'_s}{d\nu_s} \right) \frac{d^2\sigma}{d\nu'_s d\Omega'_s} \tag{28}$$

where, Ω_e is the direction of the scattering electron and ν_s is the frequency of the scattered photon. Again, $\gamma \gg 1$ also allows one to approximate the direction of the incident photon in the electron rest frame to be opposite to the direction of the electron (head-on approximation). Hence, the cosine of the angle between the incident and the scattered photon, $\cos \psi' \approx -\mu'_s$ where, μ'_s is the cosine of the angle between the direction of electron and the scattered photon. The quantities μ'_s and ν'_s are related to the corresponding quantities in the frame of emission region as

$$\mu'_s = \frac{\mu_s - \beta}{1 - \beta\mu_s} \tag{29}$$

$$\nu'_s = \nu_s \gamma (1 - \beta\mu_s) \tag{30}$$

From equations (29) and (30) we get

$$\frac{d\Omega'_s}{d\Omega_s} = \left(\frac{\nu_s}{\nu'_s} \right)^2 \tag{31}$$

Using equations (30) and (31), (28) can be expressed as

$$\frac{d^2\sigma}{d\nu_s d\Omega_s} = \delta(\Omega_s - \Omega_e) \oint d\Omega_s \left(\frac{\nu_s}{\nu'_s} \right) \frac{d^2\sigma}{d\nu'_s d\Omega'_s} \quad (32)$$

The above equation relates the differential Compton cross section between the emission region and the electron rest frame. The δ -function in equation (13) can be modified using equation (11) as

$$\delta \left[\nu'_s - \frac{\nu'_i}{1 + \frac{h\nu'_i}{m_e c^2}(1 + \mu'_s)} \right] = \frac{1}{\nu_s \left| \frac{h\nu_s}{m_e c^2} - \gamma\beta \right|} \delta \left[\mu_s - \frac{1 + \frac{h\nu'_i}{m_e c^2}(1 - \beta) - \frac{\nu'_i}{\gamma\nu_s}}{\beta - \frac{h\nu'_i}{m_e c^2}(1 - \beta)} \right] \quad (33)$$

and the differential Compton cross section in the emission region frame, equation (32), can be expressed as

$$\frac{d^2\sigma}{d\nu_s d\Omega_s} = \frac{\pi r_e^2}{\gamma\nu'_i} \delta(\Omega_s - \Omega_e) \Xi(\gamma, \nu_s, \nu'_i); \quad \frac{\nu'_i}{2\gamma} \leq \nu_s \leq \frac{2\gamma\nu'_i}{1 + 2\frac{h\nu'_i}{m_e c^2}} \quad (34)$$

where,

$$\Xi(\gamma, \nu_s, \nu'_i) = \left[y + \frac{1}{y} + \frac{\nu_s^2}{\gamma^2 \nu_i'^2 y^2} - \frac{2\nu_s}{\gamma\nu'_i y} \right] \quad \text{and} \quad y = 1 - \frac{h\nu_s}{\gamma m_e c^2} \quad (35)$$

The knowledge of differential Compton cross section lets us write the inverse Compton emissivity as

$$j_{ic}(\nu, \Omega) = c\nu \int_0^\infty d\nu_i \oint d\Omega_i \int_1^\infty d\gamma \oint d\Omega_e (1 - \beta \mu_{ie}) N_e(\gamma, \Omega_e) \frac{U_{ph}(\nu_i, \Omega_i)}{\nu_i} \frac{d^2\sigma}{d\nu d\Omega} \quad \text{erg/cm}^3/\text{s/Hz/Sr} \quad (36)$$

where, Ω_i is the direction of the incident photon, $N_e(\gamma, \Omega_e)$ is the scattering electron number density ($\text{cm}^{-3}\text{Sr}^{-1}$), $U_{ph}(\nu_i, \Omega_i)$ is the target photon energy density ($\text{erg cm}^{-3} \text{Sr}^{-1}$) and μ_{ie} is the cosine of the angle between the incident photon and the scattering electron, given by

$$\mu_{ie} = \mu_i \mu_e + \sqrt{(1 - \mu_i^2)(1 - \mu_e^2)} \cos(\phi_i - \phi_e) \quad (37)$$

with μ_i and μ_e being the cosine of the angles subtended by the incident photon and the scattering electron with the jet axis and ϕ_i and ϕ_e are the corresponding azimuthal angles. Substituting equation (34) on (36), we get

$$\begin{aligned} j_{ic}(\nu, \Omega) &= \frac{3}{8} \nu c \sigma_T \int_0^\infty d\nu_i \oint d\Omega_i \int_1^\infty d\gamma (1 - \beta \mu_{ie}) \frac{N_e(\gamma, \Omega)}{\gamma} \frac{U_{ph}(\nu_i, \Omega_i)}{\nu'_i \nu_i} \Xi(\gamma, \nu, \nu'_i) \\ &= \frac{3}{8} \nu c \sigma_T \int_0^\infty d\nu_i \oint d\Omega_i \int_1^\infty d\gamma \frac{N_e(\gamma, \Omega)}{\gamma^2} \frac{U_{ph}(\nu_i, \Omega_i)}{\nu_i^2} \Xi(\gamma, \nu, \nu'_i) \end{aligned} \quad (38)$$

where, we have used $\nu'_i = \nu_i \gamma (1 - \beta \mu_{ie})$.

In case of EC process, the energy density of the target photon in the AGN frame can be transformed to the frame of emission region using Lorentz invariance (Rybicki & Lightman 1986)

$$\frac{U_{ph}(\nu_i, \Omega_i)}{\nu_i^3} = \frac{U_{ph*}(\nu_{i*}, \Omega_{i*})}{\nu_{i*}^3} \quad (39)$$

where, $\nu_{i*} (= \nu_i \Gamma (1 + \beta_\Gamma \mu_i))$ is the frequency of the photon in the AGN frame and $\beta_\Gamma (= \sqrt{1 - 1/\Gamma^2})$ is the dimensionless bulk velocity of the emission region down the jet. Hence, for the case of an isotropic external photon field, the EC emissivity will be

$$j_{\text{ec}}(\nu, \Omega) = \frac{3}{32\pi} \frac{\nu c \sigma_T}{\Gamma^2} \int_0^\infty d\nu_{i*} \int_1^\infty d\gamma \frac{N_e(\gamma, \Omega)}{\gamma^2} \frac{U_{\text{ph}*}(\nu_{i*})}{\nu_{i*}^2} \oint d\Omega_i \frac{1}{(1 + \beta_\Gamma \mu_i)^2} \Xi(\gamma, \nu, \nu'_i) \quad (40)$$

For $\Gamma \gg 1$, relativistic beaming will cause the external photon to arrive in a direction opposite to the jet flow within a narrow cone of semi vertical angle $1/\Gamma$. Hence, $\mu_{ie} \approx -\mu$ and being independent of μ_i , Ξ can be excluded from the last solid angle integration. Here, μ is the cosine of the angle between the scattered photon and the jet direction. The integration over solid angle can then be performed analytically

$$\oint \frac{d\Omega_i}{(1 + \beta_\Gamma \mu_i)^2} = 4\pi \beta_\Gamma \Gamma^2 \quad (41)$$

and equation (40) will be reduced to

$$j_{\text{ec}}(\nu, \Omega) = \frac{3}{8} \nu c \beta_\Gamma \sigma_T \int_0^\infty d\nu_{i*} \int_1^\infty d\gamma \frac{N_e(\gamma, \Omega)}{\gamma^2} \frac{U_{\text{ph}*}(\nu_{i*})}{\nu_{i*}^2} \Xi(\gamma, \nu, \nu'_i) \quad (42)$$

For isotropic broken power-law distribution of electrons given in equation (1), we get

$$j_{\text{ec}}(\nu, \Omega) = \frac{3}{32\pi} \nu c \beta_\Gamma \sigma_T \int_0^\infty d\nu_{i*} \int_{\gamma_{\min}}^{\gamma_{\max}} d\gamma \frac{N(\gamma)}{\gamma^2} \frac{U_{\text{ph}*}(\nu_{i*})}{\nu_{i*}^2} \Xi(\gamma, \nu, \nu'_i) \quad (43)$$

and

$$\nu'_i \approx \Gamma \gamma (1 + \beta \mu) \nu_{i*} \quad (44)$$

where, we have assumed $\nu_i \approx \Gamma \nu_{i*}$ (head-on). Since μ corresponds to the viewing angle θ in the AGN frame, we can express the former in terms of the latter as

$$\begin{aligned} \mu &= \frac{\cos \theta - \beta_\Gamma}{1 - \beta_\Gamma \cos \theta} \\ &= \delta_D \Gamma (\cos \theta - \beta_\Gamma) \end{aligned} \quad (45)$$

where, $\delta_D (= [\Gamma(1 - \beta_\Gamma \cos \theta)]^{-1})$ is the Doppler factor.

For the case of monochromatic external photon field, an approximate analytical solution for EC emissivity can be obtained when the scattering process is in Thomson regime (Dermer 1995). Transformation of the scattered photon frequency from electron rest frame to emission region frame will give us $\nu_s = \nu_i \gamma^2 (1 - \beta \cos \psi)$ (Rybicki & Lightman 1986) and under head-on approximation, the differential Compton cross section in the frame of emission region can be written as

$$\frac{d^2 \sigma}{d\nu_s d\Omega_s} \approx \sigma_T \delta(\Omega_s - \Omega_e) \delta[\nu_s - \nu_i \gamma^2 (1 - \beta \mu_{ie})] \quad (46)$$

For $\Gamma \gg 1$ and $\gamma \gg 1$, the incident photons travel opposite to the jet axis and we can approximate $1 - \beta \mu_{ie} \rightarrow 1 + \mu_e$ and $U_{\text{ph}}(\nu_i, \Omega_i) \approx U_{\text{ph}}(\nu_i) \delta(\Omega_i)$. Hence, the inverse Compton emissivity equation (36) will be

$$\tilde{j}_{\text{ec}}(\nu, \Omega) \approx c \nu \sigma_T \int_0^\infty d\nu_i \int_1^\infty d\gamma (1 + \mu) N_e(\gamma, \Omega) \frac{U_{\text{ph}}(\nu_i)}{\nu_i} \delta[\nu - \nu_i \gamma^2 (1 + \mu)] \quad (47)$$

$$= \frac{1}{2} c \sigma_T \sqrt{\nu} \int_0^\infty d\nu_i \nu_i^{-3/2} \sqrt{1 + \mu} N_e \left[\sqrt{\frac{\nu}{\nu_i (1 + \mu)}}, \Omega \right] U_{\text{ph}}(\nu_i) \quad (48)$$

where, we have used the δ -function property equation (11), to perform the integration over γ . Since $U_{\text{ph}}(\nu_i) d\nu_i = \Gamma^2 U_{\text{ph}*}(\nu_{i*}) d\nu_{i*}$ and $\nu_i = \Gamma \nu_{i*}$, we get

$$\tilde{j}_{\text{ec}}(\nu, \Omega) = \frac{1}{2} c \sigma_T \sqrt{\Gamma \nu (1 + \mu)} \int_0^\infty d\nu_{i*} \nu_{i*}^{-3/2} N_e \left[\sqrt{\frac{\nu}{\Gamma \nu_{i*} (1 + \mu)}}, \Omega \right] U_{\text{ph}*}(\nu_{i*}) \quad (49)$$

For a monochromatic external photon field, $U_{\text{ph}*}(\nu_{i*}) = U_* \delta(\nu_{i*} - \bar{\nu}_*)$ at frequency $\bar{\nu}_*$, and for an isotropic electron distribution we get

$$\tilde{j}_{\text{ec}}(\nu, \Omega) = \frac{c \sigma_T U_*}{8 \pi \bar{\nu}_*} \sqrt{\frac{\Gamma \nu (1 + \mu)}{\bar{\nu}_*}} N_e \left[\sqrt{\frac{\nu}{\Gamma \bar{\nu}_* (1 + \mu)}}, \Omega \right] \quad (50)$$

and from equation (45),

$$\Gamma(1 + \mu) = \delta_D \left(\frac{\cos \theta + 1}{1 + \beta_\Gamma} \right) \quad (51)$$

It should be noted here that an external photon field of blackbody type can be approximated as a monochromatic, owing to broad spectral range of EC emissivity resulting from a power law electron distribution.

2.4 Observed Flux

The flux received by the observer due to synchrotron and inverse Compton emission processes can be obtained from their corresponding emissivities. After accounting for the relativistic Doppler boosting and cosmological effects, the observed flux⁴ at frequency ν_{obs} in the direction Ω_{obs} will be (Begelman et al. 1984; Dermer 1995)

$$F_{\text{obs}}(\nu_{\text{obs}}) = \frac{\delta_D^3 (1 + z)}{d_L^2} V j_{\text{rad}} \left(\frac{1 + z}{\delta_D} \nu_{\text{obs}}, \mu, \phi_{\text{obs}} \right) \text{ erg/cm}^2/\text{s/Hz} \quad (52)$$

where, z is the redshift of the source, d_L is the luminosity distance, V is the volume of the emission region, j_{rad} is the emissivity due to synchrotron/SSC/EC process, μ is the viewing angle measured from the frame of emission region – equation (45), and ϕ_{obs} the azimuthal angle of the observer. An approximate solution of the observed flux can be obtained by replacing the emissivity in the above equation with its corresponding analytical approximation: equation (12)/(25)/(50). It is then straight forward to obtain the relation between the source parameters and the observed fluxes due to synchrotron, SSC and EC processes as

$$F_{\text{obs}}^{\text{syn}}(\nu_{\text{obs}}) \approx \begin{cases} \mathbb{S}(z, p) \delta_D^{\frac{p+5}{2}} B^{\frac{p+1}{2}} R^3 K \nu_{\text{obs}}^{-\left(\frac{p-1}{2}\right)} & \text{for } \nu_{\text{obs}} \ll \delta_D \gamma_b^2 \nu_L / (1 + z) \\ \mathbb{S}(z, q) \delta_D^{\frac{q+5}{2}} B^{\frac{q+1}{2}} R^3 K \gamma_b^{q-p} \nu_{\text{obs}}^{-\left(\frac{q-1}{2}\right)} & \text{for } \nu_{\text{obs}} \gg \delta_D \gamma_b^2 \nu_L / (1 + z) \end{cases} \quad (53)$$

$$F_{\text{obs}}^{\text{SSC}}(\nu_{\text{obs}}) \approx \begin{cases} \mathbb{C}(z, p) \delta_D^{\frac{p+5}{2}} B^{\frac{p+1}{2}} R^4 K^2 \nu_{\text{obs}}^{-\left(\frac{p-1}{2}\right)} \log \left(\frac{\gamma_b}{\gamma_{\text{min}}} \right) & \text{for } \nu_{\text{obs}} \ll \delta_D \gamma_b^4 \nu_L / (1 + z) \\ \mathbb{C}(z, q) \delta_D^{\frac{q+5}{2}} B^{\frac{q+1}{2}} R^4 K^2 \gamma_b^{2(q-p)} \nu_{\text{obs}}^{-\left(\frac{q-1}{2}\right)} \log \left(\frac{\gamma_{\text{max}}}{\gamma_b} \right) & \text{for } \nu_{\text{obs}} \gg \delta_D \gamma_b^4 \nu_L / (1 + z) \end{cases} \quad (54)$$

$$F_{\text{obs}}^{\text{ec}}(\nu_{\text{obs}}) \approx \begin{cases} \mathbb{E}(z, p) \delta_D^{p+3} U_* \bar{\nu}_*^{\frac{p-3}{2}} R^3 K \nu_{\text{obs}}^{-\left(\frac{p-1}{2}\right)} & \text{for } \nu_{\text{obs}} \ll \delta_D \Gamma \gamma_b^2 \bar{\nu}_* / (1 + z) \\ \mathbb{E}(z, q) \delta_D^{q+3} U_* \bar{\nu}_*^{\frac{q-3}{2}} R^3 K \gamma_b^{q-p} \nu_{\text{obs}}^{-\left(\frac{q-1}{2}\right)} & \text{for } \nu_{\text{obs}} \gg \delta_D \Gamma \gamma_b^2 \bar{\nu}_* / (1 + z) \end{cases} \quad (55)$$

⁴ Quantities with subscript 'obs' are measured in the observer's frame

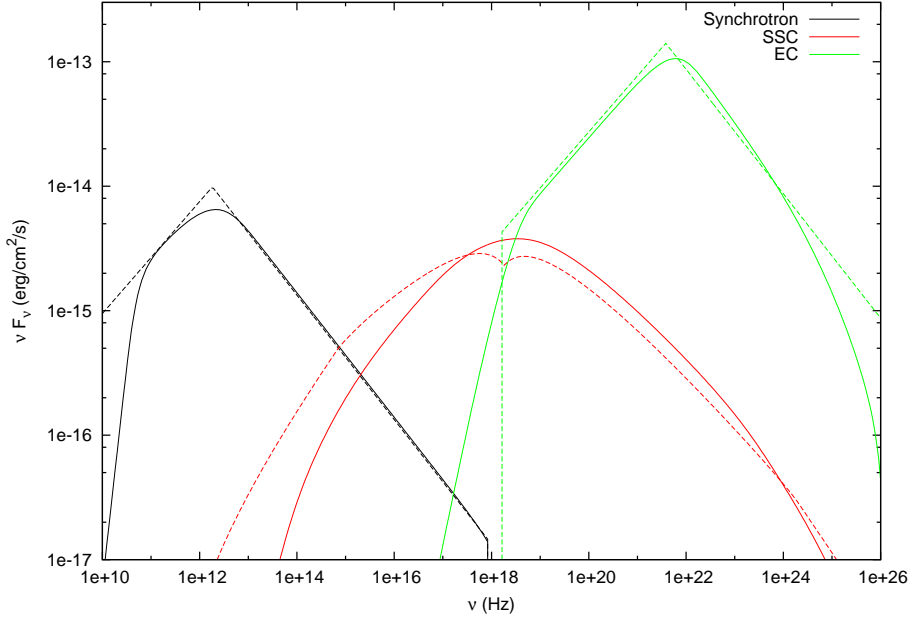


Fig. 1 The derived synchrotron, SSC and EC model spectrum (solid lines) with their approximate analytical equivalents (dashed lines). The model SED corresponds to the following source parameters: $z = 0.536$, $p = 0.55$, $q = 1.5$, $K = 1 \times 10^5$, $\gamma_{\min} = 10$, $\gamma_{\max} = 5 \times 10^5$, $\gamma_b = 10^3$, $B = 0.1$ G, $\Gamma = 10$, $\delta_D = 10$, $\bar{\nu}_* = 5.86 \times 10^{13}$ Hz equivalent to temperature 1000 K, $U_* = 7.57 \times 10^{-5}$ erg/cm³ and $R = 10^{16}$ cm

Here, \mathbb{S} , \mathbb{C} and \mathbb{E} are the quantities involving physical constants, redshift and particle index. For the EC process, we have assumed $\cos \theta \sim 1$ and $\beta_\Gamma \sim 1$. In Figure 1, we show the observed flux due to synchrotron, SSC and EC processes (solid lines) for a set of source parameters (described in the caption) along with their approximate analytical solutions (dashed lines). We find that the approximate analytical solution of fluxes closely agree with the actual numerical results (except around the peak) and hence can be used to estimate the source parameters.

2.5 Source Parameters

It is quite evident from equations (53), (54) and (55), the observed flux at any frequency basically depends upon 12 source parameters namely, K , γ_{\min} , γ_{\max} , γ_b , p , q , δ_D , Γ , B , R , $\bar{\nu}_*$ and U_* . Among these, p and q can be easily constrained from observed spectral indices since, the spectral indices due to synchrotron and inverse Compton processes will be $(p - 1)/2$ and $(q - 1)/2$ (section Section 2.4). Now, as the low energy end of the blazar SED is affected by synchrotron self absorption and the high energy tail by Klein-Nishina effects (or often unknown), it is hard to estimate the parameters γ_{\min} and γ_{\max} . However, on the basis of shock acceleration theory, one can impose a constrain on γ_{\min} such that $\gamma_{\min} \gtrsim \Gamma$ (Kino et al. 2002). On the other hand, γ_{\max} is a weak parameter and can be chosen to reproduce the highest energy of the gamma ray photon observed. Thus, after assigning a convenient choice for γ_{\min} and γ_{\max} , we are finally left with 8 parameters which are to be determined from observations.

A good spectral information at optical/UV/X-ray energies will let us identify the synchrotron peak frequency ($\nu_{\text{sp,obs}}$) in the blazar SED and the same can be expressed in terms of the source parameters

as

$$\nu_{\text{sp,obs}} = \left(\frac{\delta_D}{1+z} \right) \gamma_b^2 \nu_L \quad (56)$$

Similarly, if one can identify the SSC and the EC peak from the high energy spectrum, then the SSC peak can be expressed as

$$\nu_{\text{sscp,obs}} = \left(\frac{\delta_D}{1+z} \right) \gamma_b^4 \nu_L \quad (57)$$

and the EC peak

$$\nu_{\text{ecp,obs}} = \left(\frac{\delta_D \Gamma}{1+z} \right) \gamma_b^2 \bar{\nu}_* \quad (58)$$

If the external photon field is assumed to be a blackbody, illuminated by the accretion disk, then $U_{\text{ph}*}$ and $\bar{\nu}_*$ can be related as

$$\bar{\nu}_* = 2.82 f_{\text{ext}} \frac{K_B}{h} \left(\frac{c}{4\sigma_{SB}} \int U_{\text{ph}*}(\nu_{i*}) d\nu_{i*} \right)^{1/4} \quad (59)$$

where, K_B is the Boltzmann constant, σ_{SB} is the Stefan-Boltzmann constant, $U_{\text{ph}*}(\nu_{i*})$ is the black-body energy density at frequency ν_{i*} and f_{ext} is the covering factor describing the fraction of external photons participating in the inverse Compton process. Besides these, we can also express the magnetic field energy density (U_B) in terms of electron energy density (U_e) as

$$U_B = \eta U_e \quad (60)$$

where,

$$U_B = \frac{B^2}{8\pi} \text{ erg/cm}^3 \quad \text{and} \quad U_e = m_e c^2 \int_{\gamma_{\min}}^{\gamma_{\max}} \gamma N(\gamma) d\gamma \text{ erg/cm}^3$$

Here, $\eta \approx 1$ corresponds to the equipartition condition indicating total energy of the system to be minimum (Pacholczyk 1970). Hence, the knowledge of $\nu_{\text{sp,obs}}$, $\nu_{\text{sscp,obs}}$, $\nu_{\text{ecp,obs}}$ and the fluxes at Optical (Synchrotron; equation (53)), X-ray (SSC; equation (54)) and gamma ray (EC; equation (55)), along with equations (59) and (60), can in principle, let one estimate the remaining 8 source parameters by solving the corresponding coupled equations.

In case of simple models involving only synchrotron and SSC alone (for e.g. SED of many BL Lac objects), the total number of source parameters reduces to 9 since, the parameters Γ , $\bar{\nu}_*$ and U_* will be redundant. Leaving the electron spectral indices, γ_{\min} and γ_{\max} , we will be left with only 5 parameters which can be estimated from the set of coupled equations (53), (54), (56), (57) and (60). Non-availability of any of these observables may not allow to estimate an unique set of parameters and one needs to assume certain parameters a priori. Alternatively, one can add other observable features (e.g. variability timescale, synchrotron self absorption break frequency, transition frequency from dominant synchrotron emission to inverse Compton etc) to constrain the model and obtain a unique set of source parameters.

3 XSPEC SPECTRAL FIT

We developed numerical codes to calculate the emissivities corresponding to synchrotron, SSC and EC emission processes, which are then used to estimate the observed fluxes after accounting for the relativistic and cosmological transformations. The codes are optimized by incorporating quadrature integrations

and different interpolation schemes to reduce the run time⁵. These codes are then added as additive local models to the XSPEC package following the standard prescription⁶. We choose the parameters of the combined XSPEC models as, the electron spectral indices p and q , minimum and the maximum electron energies γ_{\min} and γ_{\max} , synchrotron peak frequency $\nu_{\text{sp,obs}}$, SSC peak frequency $\nu_{\text{sscp,obs}}$, EC peak frequency $\nu_{\text{ecp,obs}}$, synchrotron flux $F_{\text{obs}}^{\text{syn}}$ at a reference frequency $\nu_{\text{syn,obs}}^{\text{ref}}$, SSC flux $F_{\text{obs}}^{\text{sssc}}$ at a reference frequency $\nu_{\text{ssc,obs}}^{\text{ref}}$, EC flux $F_{\text{ec,obs}}^{\text{ec}}$ at a reference frequency $\nu_{\text{ec,obs}}^{\text{ref}}$ and equipartition factor η . To extend the application of the code to fit the SED of misaligned AGNs, we also include an option to incorporate large viewing angles. This is achieved by considering the ratio of the Doppler factor δ_D to the bulk Lorentz factor Γ as an additional parameter. The advantage of providing observed parameters as input to the XSPEC codes will let us to avoid the uncertainty regarding the correct choice of initial guess parameters as well as facilitate a faster convergence. These observed parameters are then converted into source parameters within the code by solving the approximate coupled equations and other conditions described in the earlier section. Consistently, the same procedure is then used to extract the best fit source parameters from the fitted observational quantities.

3.1 Spectral fitting of 3C 279

To further study and validate the proposed broadband spectral fitting algorithm using XSPEC, we choose the well studied FSRQ, 3C 279 ($z = 0.536$), as a test case. We select the flaring epoch of 3C 279, during March-April 2014, when the source was observed to be very bright in gamma rays. This huge gamma ray flare was witnessed by *Fermi* gamma ray telescope and was simultaneously monitored at X-ray energies by *Swift-XRT* and in UV/optical by *Swift-UVOT*, *SMARTS* and *Steward* observatories, thereby providing an unprecedented multi wavelength data (Paliya et al. 2015). In Figure 2, we show the observed SED corresponding to the highest gamma ray flux state (2-8 April 2014) encountered during this flaring episode.

Earlier studies on the broadband SED of 3C 279 suggests, substantial contribution of synchrotron, SSC and EC processes and this further assures that this source can be a right choice for testing the proposed spectral fitting algorithm (Sahayanathan & Godambe 2012; Hartman et al. 2001). The justification behind this inference is that the observed X-ray and gamma ray fluxes from 3C 279 cannot be interpreted under single emission process like SSC or EC, as it demands a magnetic field that deviate largely from the equipartition condition. In addition, detection of 3C 279 at very high energy gamma rays (VHE) with relatively hard spectrum indicates, the EC process to be dominated by scattering of infrared photons from the obscuring torus (EC/IR), rather than the Lyman alpha line emission from the broad line emitting regions (EC/BLR) (Ghisellini & Tavecchio 2009). For the flaring period under consideration, no significant detection of VHE emission was reported from the source and hence, we cannot assert that the gamma ray emission to be an outcome of EC/IR or EC/BLR processes. However, it can be shown that the observed fluxes at optical, X-ray and gamma ray energies support EC/IR interpretation of the high energy emission (Shah et al. 2017).

Though the flare under consideration was simultaneously monitored at optical, X-ray and gamma ray energies, non-availability of lower frequency observation at microwave/IR prevents us from estimating $\nu_{\text{sp,obs}}$. Similarly, $\nu_{\text{sscp,obs}}$ also remains uncertain since the X-ray spectra do not show any signature of a peak. A lack of these informations causes a deficit in the number of observables and thereby, prevents us from obtaining a unique set of source parameters. Thus, we fix the values of $\nu_{\text{sp,obs}}$ and $\nu_{\text{sscp,obs}}$ to appropriate values to obtain meaningful source parameters. Accordingly, these quantities are fixed at $\nu_{\text{sp,obs}} = 3.8 \times 10^{13}$ Hz and $\nu_{\text{sscp,obs}} = 7.6 \times 10^{19}$ Hz, and we fitted the spectrum to obtain the rest of the observables. Further, to allow for the uncertainties regarding the emission models, a systematic error of 10% was applied evenly on all the emission models in addition to the uncertainties

⁵ Typically, the runtime for 1000 iterations of generating 100 flux points sampled logarithmically over a broadband SED, spanning over radio to gamma ray energies, and involving synchrotron, SSC and EC emission processes, on an Intel i5 machine (3.3 GHz \times 4 processors) with 8 GB RAM, is 4 mins approximately.

⁶ <http://heasarc.gsfc.nasa.gov/docs/xanadu/xspec/manual/manual.html>

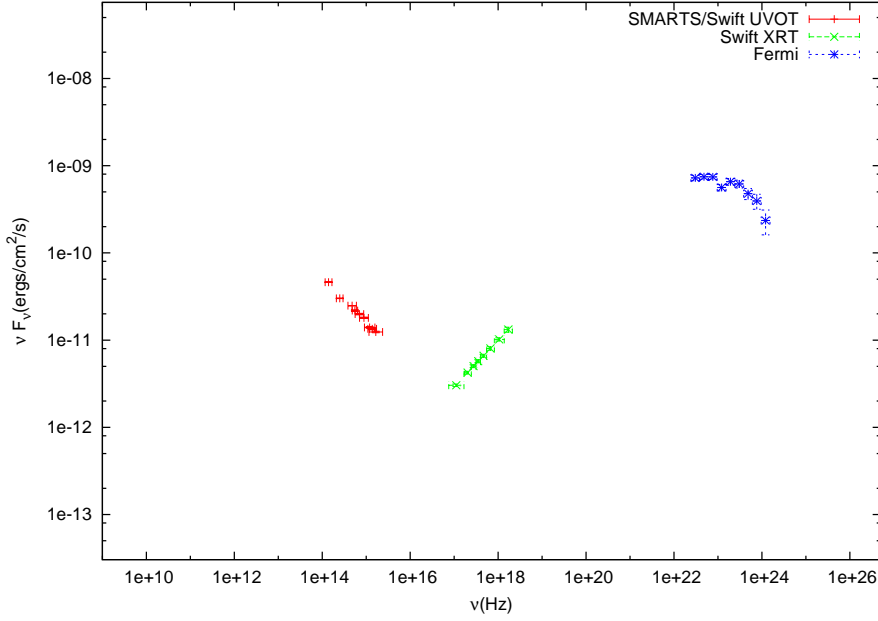


Fig. 2 Broadband SED of 3C 279 during its gamma ray high state on 2-8 April 2014. The source was simultaneously observed at optical/UV (*SMARTS*, *Swift-UVOT*), X-ray (*Swift-XRT*) and gamma ray (*Fermi*) energies (Paliya et al. 2015).

in the observed fluxes. Finally, the best fit spectrum along with the residual, resulting from the present study, is shown in Figure 3. In Table 1, we give the best fit observational quantities corresponding to a minimum reduced chi square of $\chi_{red} = 0.8$ for 20 degrees of freedom. The 1-sigma confidence range of these quantities are obtained by scanning the parameter space around this minima. In Figures 4 and 5, we show the contour plots between different quantities for 1- σ ($\Delta\chi^2 = 2.3$) and 2- σ ($\Delta\chi^2 = 4.61$) confidence levels.

The knowledge of the best fit observational quantities can be inverted back to obtain the corresponding source parameters using the approximate analytical expression described earlier (Section 2.4 and Section 2.5). Since the emission codes use the same expressions to derive the source parameters and the emissivities, the resulting source parameters will also be the best fit values giving rise to same χ^2 . In Table 2, we give the source parameters derived from the best fit observable quantities, mentioned in Table 1. To obtain the confidence range, we again use the approximate analytical expressions to extract the source parameter range from the observable parameter space. However to be consistent with the freezing of the observed quantities $\nu_{sp,obs}$ and $\nu_{sscp,obs}$, we fix the source parameters $\bar{\nu}_* = 6 \times 10^{13}$ Hz (corresponding to $T_* \approx 1000$ K) and $\gamma_b = 1.4 \times 10^3$. In Figure 6 and 7, we show the contour plots between the rest of the source parameters namely, δ_D , K , U_* , B and R , corresponding to 1- σ and 2- σ confidence levels.

4 DISCUSSION

The blazar spectral fitting algorithm demonstrated in the present work provides a convenient way to understand the different emission processes as well as to extract the parameters governing the source. The error ellipses between different parameters (Figures 4, 5, 6 and 7), indicate the allowed ranges and the possible correlations between the parameters. Availability of a well sampled SED of a source at synchrotron, SSC and EC spectral components, will let one to perform the fitting with more free

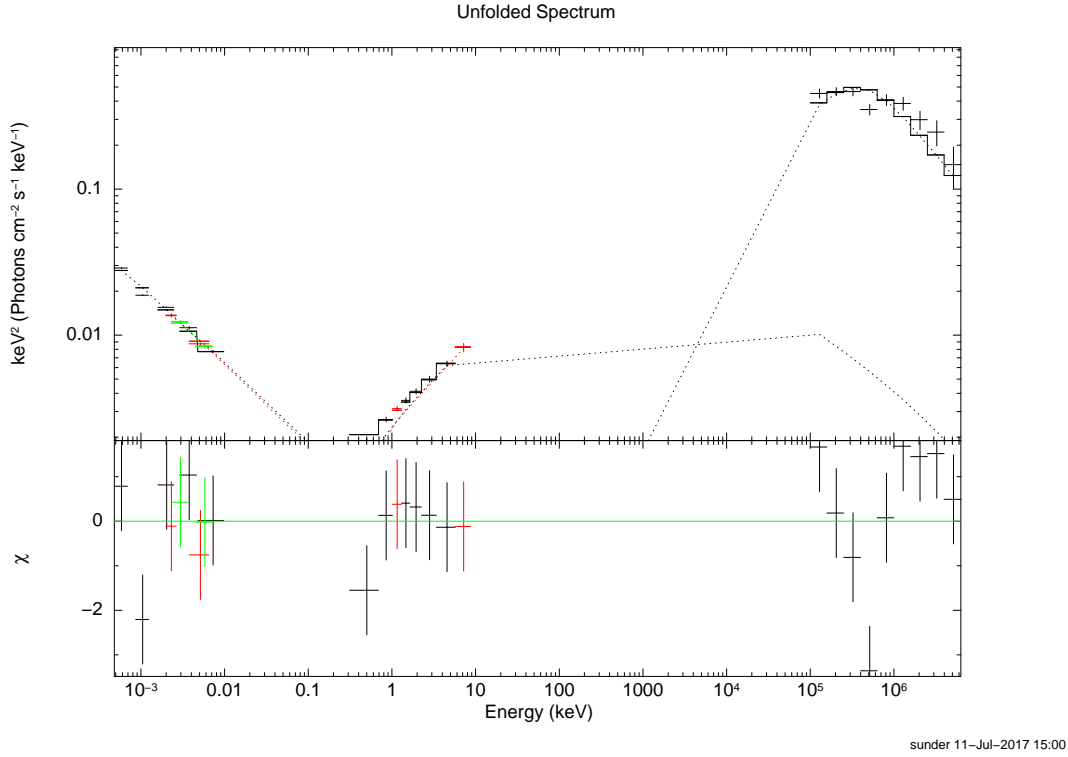


Fig. 3 XSPEC spectral fit of the broadband SED of 3C 279 using synchrotron, SSC and EC processes.

parameters. This in turn, will help us to understand the physical condition of the source during that particular observation.

Besides providing the best fit parameters, the algorithm developed in this work, will also help us to eliminate the degenerate parameters. Lack of information about the observed quantities, like peak frequencies, fluxes due to different emission processes, etc., will lead to degenerate source parameters irrespective of having a well sampled data. In conventional algorithms, where fitting is performed directly on the source parameters, this degeneracy between the parameters cannot be anticipated and can lead to misconceptions. For example, a spectral fit similar to the one shown in Figure 3 can be obtained for a different choice of $\nu_{sp,obs}$. However, this will give rise to a different set of source parameters and particularly the target photon temperature. In such cases, one cannot differentiate between the target photon field responsible for the gamma ray emission through EC scattering. The knowledge of the synchrotron peak frequency can, thereby, help us in removing this degeneracy. Alternatively, detection of the source at VHE, can also impose certain constraints on the temperature of the external photon field (Ghisellini & Tavecchio 2009). Nevertheless, the constraints as well as the degeneracy of the parameters depend on the choice of the physical model, the initial assumptions and the quality of the observed SED.

The procedure of extracting the physical parameters of the 3C 279 using approximate analytical expressions, without statistical fitting, was also demonstrated by Sahayanathan & Godambe (2012), during the flare observed on 2006. They show the high energy emission can be successfully explained by the EC scattering of the IR photons and the parameters quoted are comparable to the one presented here. The observed SED used in the present work was taken from Paliya et al. (2015) where, the broadband SED of the same epoch was modelled using synchrotron, SSC, EC/IR and EC/BLR emission processes. The quoted parameters differ from the ones obtained here since, the inclusion of additional emission process

Table 1 XSPEC fit result

Observable	Symbol	Value
Low energy Particle index	p	1.64
High energy Particle index	q	4.09
Synchrotron peak frequency ^{f} (Hz)	ν_{syn}^p	3.83×10^{13}
SSC peak frequency ^{f} (Hz)	ν_{ssc}^p	7.65×10^{19}
EC peak frequency (Hz)	ν_{ec}^p	5.0×10^{22}
Synchrotron Flux (erg/cm ² /s)	F^{syn}	3.23×10^{-11}
Synchrotron reference frequency* (Hz)	$\nu_{\text{syn}}^{\text{ref}}$	2.4×10^{14}
SSC Flux (erg/cm ² /s)	F^{syn}	9.88×10^{-12}
SSC reference frequency* (Hz)	$\nu_{\text{ssc}}^{\text{ref}}$	4.79×10^{17}
EC Flux (erg/cm ² /s)	F^{syn}	3.44×10^{-10}
EC reference frequency* (Hz)	$\nu_{\text{ec}}^{\text{ref}}$	4.79×10^{23}
Equipartition factor ^{f}	η	0.1
Ratio of Doppler to Lorentz factor ^{f}	δ_D/Γ	1
Minimum electron energy ^{f}	γ_{min}	40
Maximum electron energy ^{f}	γ_{max}	10^6

Notes: Best fit observable quantities/source parameters of 3C 279, during the gamma ray flare on 2014, obtained using XSPEC emission models developed in this work. Quantities with superscript f are fixed and not included in the fitting. The reference frequencies, denoted by superscript *, are the ones at which the observed fluxes are fitted.

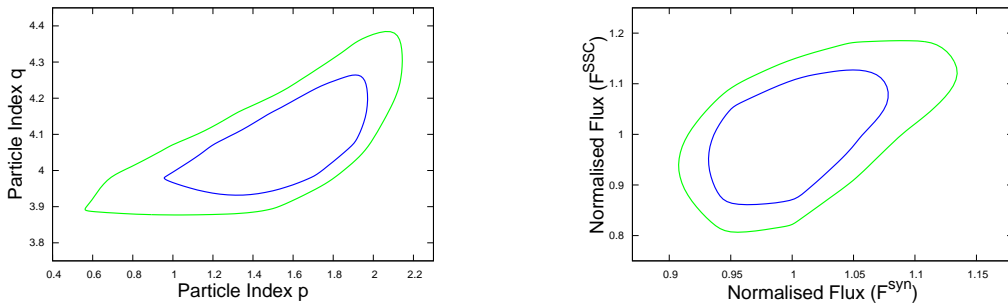


Fig. 4 The 1- σ (blue) and 2- σ (green) confidence interval between the broken power law electron spectral indices p and q (left), and the synchrotron and SSC fluxes normalised to its best fit flux (right).

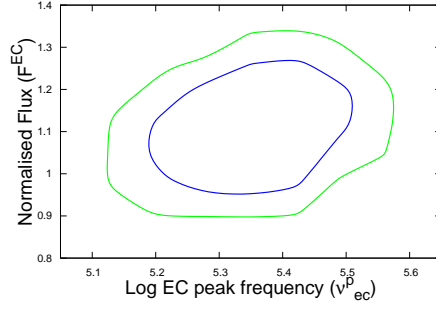


Fig. 5 The 1- σ (blue) and 2- σ (green) confidence interval between the EC peak frequency and the normalised EC flux.

Table 2 Best fit source parameters

Observable ^a	Symbol	Value
Low energy Particle index	p	1.64
High energy Particle index	q	4.09
Particle normalisation (cm^{-3})	K	2.45×10^3
Break Lorentz factor	γ_b	1.41×10^3
Minimum electron Lorentz factor	γ_{\min}	40
Maximum electron Lorentz factor	γ_{\max}	1.0×10^6
Bulk Lorentz factor	Γ	25.45
Doppler Factor	δ_D	25.45
Magnetic Field (G)	B	0.41
Emission region size (cm)	R	2.36×10^{16}
Target photon frequency (Hz)	ν_*	5.95×10^{13}
Target photon energy density (erg/cm^3)	U_*	1.88×10^{-4}

Notes: The source parameters corresponding to the best fit observable quantities given in Table 1. These values are extracted using the same approximate analytical expressions used in the XSPEC emission models.

will increase the number of parameters which cannot be effectively constrained using the limited information available. Nevertheless, the SEDs during the flaring state and quiescent state can be reproduced satisfactorily under these emission models. Yan et al. (2016) employed Markov chain Monte Carlo technique to build 14 bright SEDs of 3C 279. Their emission model is similar to the one used by Paliya et al. (2015); however, they are able to provide the confidence ranges of the obtained parameters corresponding to the adapted Bayesian statistics. Zheng & Yang (2016) used an inhomogeneous jet model (Potter & Cotter 2012) to model the SED of 3C 279. The jet is assumed to be conical and the source parameters are chosen to vary along the jet. Using this model they were able to reproduce the broadband SEDs of the source during 2008 and 2010.

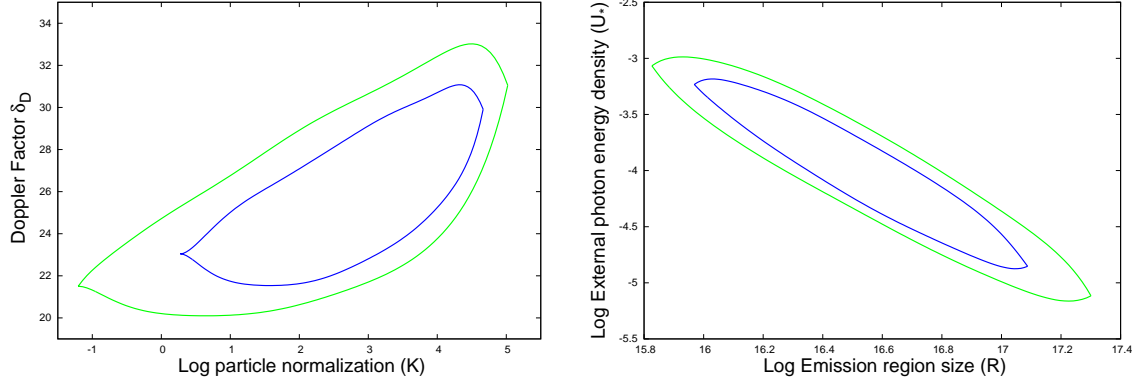


Fig. 6 The 1- σ (blue) and 2- σ (green) confidence interval between the particle normalisation K (in log) and the Doppler factor δ is shown at the left; whereas, the one at right is between emission region size R (in log) and the external photon energy density U_* (in log).

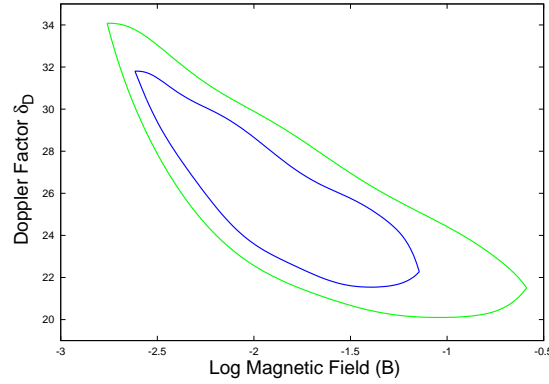


Fig. 7 The 1- σ (blue) and 2- σ (green) confidence interval between the magnetic field B (in log) and the Doppler factor δ .

Having developed an algorithm to perform a spectral fitting using synchrotron, SSC and EC processes, the present work can be easily extended to include more than one EC processes (Dermer et al. 2014) or reduced to a simple model involving only synchrotron and SSC processes. For the latter case, the reduction in the number of source parameters (Section 2.5) and omission of the EC component of the code will eventually led to faster convergence of the fitting process. Besides the observational quantities used in this work for fitting the data, the variability time scale can also play an important role in constraining the parameters. Knowledge of the variability time scale, t_{var} , can effectively constrain the size of the emission region as

$$R \lesssim \frac{c\delta_D\Delta t_{\text{obs}}}{c} \quad (61)$$

Inclusion of this will allow us to omit the equipartition condition (equation (60)) for parameter estimation. On the other hand, the obtained parameters can also be used to verify this condition or to constrain γ_{min} .

The treatment described in this work can be modified/improved further by including other observational features of blazar SEDs. For example, one can include the synchrotron self absorption frequency

which can effectively constrain the magnetic field. Similarly, transition frequency where the synchrotron emissivity is equal to the inverse Compton emissivity can be an additional information. This along with other equations can be useful in identifying the electron energies responsible for the emission at a given frequency. This is expected to play an important role in understanding the evolution of the light curves at different frequencies, the temporal evolution of the particle distribution and the dynamics of the AGN jets.

5 CONCLUSION

In the present work, we develop a statistical fitting procedure of the broadband spectrum of blazars, considering synchrotron, SSC and EC emission mechanisms. To avoid the difficulty of choosing the initial guess values as well as to warrant a faster convergence, we fit the observed quantities, like the peak frequencies, fluxes due to different emission processes etc, instead of the source parameters governing the observed spectrum. The source parameters are then calculated using approximate analytical solutions of the various emissivities. Finally, we test and validate the procedure by fitting the simultaneous broadband observation of the FSRQ, 3C 279, during its gamma ray high state. We show that the proposed spectral fitting procedure is successful in extracting most of the parameters of the source. In addition, the proposed methodology will be particularly important for the ongoing/upcoming multiwavelength campaigns which can effectively probe blazars at various energies and provide substantial information necessary to extract the probable physical scenario of the source.

References

- Abdo, A. A., Ackermann, M., Agudo, I., et al. 2010, *ApJ*, 716, 30 [1](#)
- Abdo, A. A., Ackermann, M., Ajello, M., et al. 2011, *ApJ*, 736, 131 [2](#)
- Aleksić, J., Ansoldi, S., Antonelli, L. A., et al. 2015, *A&A*, 573, A50 [2](#)
- Antonucci, R. 1993, *ARA&A*, 31, 473 [1](#)
- Arnaud, K. A. 1996, in *Astronomical Society of the Pacific Conference Series*, Vol. 101, *Astronomical Data Analysis Software and Systems V*, ed. G. H. Jacoby & J. Barnes, 17 [3](#)
- Begelman, M. C., Blandford, R. D., & Rees, M. J. 1984, *Reviews of Modern Physics*, 56, 255 [10](#)
- Begelman, M. C., & Sikora, M. 1987, *ApJ*, 322, 650 [2](#)
- Bhagwan, J., Gupta, A. C., Papadakis, I. E., & Wiita, P. J. 2014, *MNRAS*, 444, 3647 [2](#)
- Błażejowski, M., Sikora, M., Moderski, R., & Madejski, G. M. 2000, *ApJ*, 545, 107 [2](#)
- Blumenthal, G. R., & Gould, R. J. 1970, *Reviews of Modern Physics*, 42, 237 [2](#), [5](#)
- Boettcher, M., Mause, H., & Schlickeiser, R. 1997, *A&A*, 324, 395 [2](#)
- Carnerero, M. I., Raiteri, C. M., Villata, M., et al. 2015, *MNRAS*, 450, 2677 [2](#)
- Chiaberge, M., & Ghisellini, G. 1999, *MNRAS*, 306, 551 [4](#)
- Dermer, C. D. 1995, *ApJ*, 446, L63 [9](#), [10](#)
- Dermer, C. D., Cerruti, M., Lott, B., Boisson, C., & Zech, A. 2014, *ApJ*, 782, 82 [18](#)
- Dermer, C. D., & Menon, G. 2009, *High Energy Radiation from Black Holes: Gamma Rays, Cosmic Rays, and Neutrinos* [7](#)
- Dermer, C. D., & Schlickeiser, R. 1993, *ApJ*, 416, 458 [2](#), [7](#)
- Dermer, C. D., Schlickeiser, R., & Mastichiadis, A. 1992, *A&A*, 256, L27 [2](#)
- Dondi, L., & Ghisellini, G. 1995, *MNRAS*, 273, 583 [1](#)
- Francis, P. J., Hewett, P. C., Foltz, C. B., et al. 1991, *ApJ*, 373, 465 [1](#)
- Ghisellini, G., & Madau, P. 1996, *MNRAS*, 280, 67 [2](#)
- Ghisellini, G., & Maraschi, L. 1989, *ApJ*, 340, 181 [2](#)
- Ghisellini, G., & Svensson, R. 1991, *MNRAS*, 252, 313 [4](#)
- Ghisellini, G., & Tavecchio, F. 2009, *MNRAS*, 397, 985 [2](#), [13](#), [15](#)
- Hartman, R. C., Böttcher, M., Aldering, G., et al. 2001, *ApJ*, 553, 683 [13](#)
- Jones, F. C. 1968, *Physical Review*, 167, 1159 [5](#)
- Kang, S.-J., Chen, L., & Wu, Q. 2014, *ApJS*, 215, 5 [2](#)

- Kino, M., Takahara, F., & Kusunose, M. 2002, *ApJ*, 564, 97 [11](#)
- Konigl, A. 1981, *ApJ*, 243, 700 [2](#)
- Kushwaha, P., Sahayanathan, S., Lekshmi, R., et al. 2014, *MNRAS*, 442, 131 [2](#)
- Kushwaha, P., Sahayanathan, S., & Singh, K. P. 2013, *MNRAS*, 433, 2380 [2](#)
- Liu, H. T., & Bai, J. M. 2006, *ApJ*, 653, 1089 [1](#)
- Malmrose, M. P., Marscher, A. P., Jorstad, S. G., Nikutta, R., & Elitzur, M. 2011, *ApJ*, 732, 116 [1](#)
- Mankuzhiyil, N., Ansoldi, S., Persic, M., & Tavecchio, F. 2011, *ApJ*, 733, 14 [2](#)
- Marscher, A. P., & Gear, W. K. 1985, *ApJ*, 298, 114 [2](#)
- Melia, F., & Konigl, A. 1989, *ApJ*, 340, 162 [2](#)
- Melrose, D. B. 1980, *Plasma astrophysics. Nonthermal processes in diffuse magnetized plasmas - Vol.1: The emission, absorption and transfer of waves in plasmas; Vol.2: Astrophysical applications* [4](#)
- Pacholczyk, A. G. 1970, *Radio astrophysics. Nonthermal processes in galactic and extragalactic sources* [12](#)
- Padovani, P., Giommi, P., Landt, H., & Perlman, E. S. 2007, *ApJ*, 662, 182 [1](#)
- Paliya, V. S., Sahayanathan, S., & Stalin, C. S. 2015, *ApJ*, 803, 15 [2](#), [13](#), [14](#), [15](#), [17](#)
- Potter, W. J., & Cotter, G. 2012, *MNRAS*, 423, 756 [17](#)
- Press, W. H., Teukolsky, S. A., Vetterling, W. T., & Flannery, B. P. 1992, *Numerical recipes in FORTRAN. The art of scientific computing* [2](#)
- Rani, B., Lott, B., Krichbaum, T. P., Fuhrmann, L., & Zensus, J. A. 2013, *A&A*, 557, A71 [2](#)
- Rybicki, G. B., & Lightman, A. P. 1986, *Radiative Processes in Astrophysics*, 400 [2](#), [4](#), [8](#), [9](#)
- Sahayanathan, S., & Godambe, S. 2012, *MNRAS*, 419, 1660 [2](#), [3](#), [5](#), [6](#), [13](#), [15](#)
- Sambruna, R. M., Maraschi, L., & Urry, C. M. 1996, *ApJ*, 463, 444 [1](#)
- Shah, Z., Sahayanathan, S., Mankuzhiyil, N., et al. 2017, *arXiv:1705.06185* [13](#)
- Shu, F. H. 1991, *The physics of astrophysics. Volume 1: Radiation*. [4](#)
- Sikora, M., Begelman, M. C., & Rees, M. J. 1994, *ApJ*, 421, 153 [2](#)
- Sinha, A., Shukla, A., Misra, R., et al. 2015, *A&A*, 580, A100 [2](#)
- Sinha, A., Shukla, A., Saha, L., et al. 2016, *A&A*, 591, A83 [2](#)
- Tavecchio, F., Maraschi, L., & Ghisellini, G. 1998, *ApJ*, 509, 608 [2](#)
- Urry, C. M., & Padovani, P. 1995, *PASP*, 107, 803 [1](#)
- Yan, D., He, J., Liao, J., Zhang, L., & Zhang, S.-N. 2016, *MNRAS*, 456, 2173 [17](#)
- Zhang, J., Liang, E.-W., Zhang, S.-N., & Bai, J. M. 2012, *ApJ*, 752, 157 [2](#)
- Zhang, J., Sun, X.-N., Liang, E.-W., et al. 2014, *ApJ*, 788, 104 [2](#)
- Zhang, J., Xue, Z.-W., He, J.-J., Liang, E.-W., & Zhang, S.-N. 2015, *ApJ*, 807, 51 [2](#)
- Zhang, J., Zhang, S.-N., & Liang, E.-W. 2013, *ApJ*, 767, 8 [2](#)
- Zheng, Y. G., & Yang, C. Y. 2016, *MNRAS*, 457, 3535 [17](#)